Supplementary material

1. Dronkers' approach

The Chebyshev polynomials approach of Dronkers (1964) also provides a way to account for river discharge. It leads to a friction term expressed as:

$$F_D = \frac{1}{K^2 \overline{h}^{4/3} \pi}\left(p_0 \upsilon^2 + p_1 \upsilon U + p_2 U^2 + p_3 U^3 / \upsilon\right), \tag{S1.1}$$

where p_i (i=0, 1, 2, 3) are the Chebyschev coefficients according to Dronkers (1964, p. 301), which depend on φ through α in Eq. (19). The subscript D stands for Dronkers. They can be expressed as:

$$p_0 = -\frac{7}{120}\sin(2\alpha) + \frac{1}{24}\sin(6\alpha) - \frac{1}{60}\sin(8\alpha), \tag{S1.2}$$

$$p_1 = \frac{7}{6}\sin(\alpha) - \frac{7}{30}(3\alpha) - \frac{7}{30}\sin(5\alpha) + \frac{1}{10}\sin(7\alpha), \tag{S1.3}$$

$$p_2 = \pi - 2\alpha + \frac{1}{3}\sin(2\alpha) + \frac{19}{30}\sin(4\alpha) - \frac{1}{5}\sin(6\alpha), \tag{S1.4}$$

$$p_3 = \frac{4}{3}\sin(\alpha) - \frac{2}{3}\sin(3\alpha) + \frac{2}{15}\sin(5\alpha), \tag{S1.5}$$

The coefficients p_1, p_2 and p_3 determine the magnitude of linear, quadratic and cubic frictional interaction, respectively. It appears that the values of p_0 are small with respect to the values of the other coefficients; thus this term can usually be neglected. The coefficients p_1 and p_3 decrease with increasing φ until they converge to 0 for $\varphi > 1$. For $\varphi \geq 1$, p_0=p_1=p_3=0 and p_2=-π, so that the friction term becomes $F_D = U^2 / \left(K^2 \overline{h}^{4/3}\right)$. If $\varphi = 1$, p_0=p_2=0, p_1=16/15 and p_3=32/15, so that equation (S1.1) reduces to

$$F_D = \frac{16}{15\pi}\frac{\upsilon^2}{K^2 \overline{h}^{4/3}}\left[\frac{U}{\upsilon} + 2\left(\frac{U}{\upsilon}\right)^3\right]. \tag{S1.6}$$

Using Dronkers' friction term Eq. (S1.1) in the envelope method described in the Appendix A, we are able to derive the following expression:

$$\Gamma_D = \frac{1}{\pi}\left[p_1 - 2p_2\varphi + p_3\varphi^2\left(3 + \left(\frac{\mu\lambda}{\varphi}\right)^2\right)\right]. \tag{S1.7}$$

Also in this case, the periodic variation of the depth in the friction term can be accounted for by setting κ=1 in the expression provided in Table 3.

2. Godin's approach

For tidal river applications (e.g., the upper Saint Lawrence river), Godin (1991, 1999) showed that an accurate approximation of the friction term can be obtained by using only the first and third order terms of the dimensionless velocity. Adopting this approximation yields:

$$F_G = \frac{16}{15\pi}\frac{V^2}{K^2 \overline{h}^{4/3}}\left[\frac{U}{U'} + 2\left(\frac{U}{U'}\right)^3\right], \tag{S2.1}$$

where subscript *G* stands for Godin, and *U'* is defined as

$$U' = \upsilon + U_r. \tag{S2.2}$$

Equation (S2.1) is very similar to Eq. (S1.6), the difference being that in Dronkers' approach U is made dimensionless by the tidal velocity amplitude υ, while Godin does this with the maximum possible velocity U'.

Applying equation (S2.1) in the same procedure as described in Appendix A for the Lorentz's case, we readily obtain the following expression:

$$\Gamma_G = G_0 + G_1 \left(\mu\lambda\right)^2, \tag{S2.3}$$

with

$$G_0 = \frac{16}{15\pi}\frac{1+2\varphi+7\varphi^2}{1+\varphi}, \quad G_1 = \frac{32}{15\pi}\frac{1}{1+\varphi}. \tag{S2.4}$$

If U_r=0 (implying that $U'=\upsilon$) G_0=16/(15π) and G_1=32/(15π), and the method is identical to Dronkers' expression Eq. (S1.7).

The expression accounting for the periodic variation of the depth in the denominator of the friction term is reported in Table 3, where

$$G_2 = \frac{128}{15\pi}\frac{\varphi}{1+\varphi}, \quad G_3 = \frac{64}{15\pi}\frac{\frac{1}{3}\varphi+\frac{2}{3}\varphi^2+\varphi^3}{1+\varphi}. \tag{S2.5}$$

3. More detailed comparison between analytical solutions against numerical results

The tidally averaged friction can be estimated by:

$$\overline{\frac{V|V|}{K^2h^{4/3}}} = \frac{1}{2}\left[\frac{V_{HW}|V_{HW}|}{K^2\left(\bar{h}+\eta\right)^{4/3}} + \frac{V_{LW}|V_{LW}|}{K^2\left(\bar{h}-\eta\right)^{4/3}}\right]. \tag{S3.1}$$

With regard to hybrid model, the friction at HW is given by:

$$\frac{V_{HW}|V_{HW}|}{K^2\left(\bar{h}+\eta\right)^{4/3}} = \pm\frac{2}{3}\frac{\left(\upsilon\sin\varepsilon - U_r\right)^2}{K^2\left(\bar{h}+\eta\right)^{4/3}} + \frac{1}{3}\frac{L_0\upsilon^2/4 + L_1\upsilon^2\sin\varepsilon/2}{K^2\left(\bar{h}+\eta\right)^{4/3}}, \tag{S3.2}$$

where the first term on the right-hand side has a positive value if $\upsilon \sin\varepsilon > U_r$ and a negative value if $\upsilon \sin\varepsilon < U_r$.

Similarly, the friction at LW reads:

$$\frac{V_{LW}|V_{LW}|}{K^2\left(\bar{h}-\eta\right)^{4/3}} = -\frac{2}{3}\frac{\left(\upsilon\sin\varepsilon + U_r\right)^2}{K^2\left(\bar{h}-\eta\right)^{4/3}} + \frac{1}{3}\frac{L_0\upsilon^2/4 - L_1\upsilon^2\sin\varepsilon/2}{K^2\left(\bar{h}-\eta\right)^{4/3}}. \tag{S3.3}$$

To illustrate the capability of the proposed analytical model when considering the effect of river discharge, Figs. S1—S8 present some comparisons between analytical solutions and numerical results for different sets of parameters (with K=40 and 70 $m^{1/3}s^{-1}$, b=352 and 141 km, ζ_0=0.2 and 0.5).

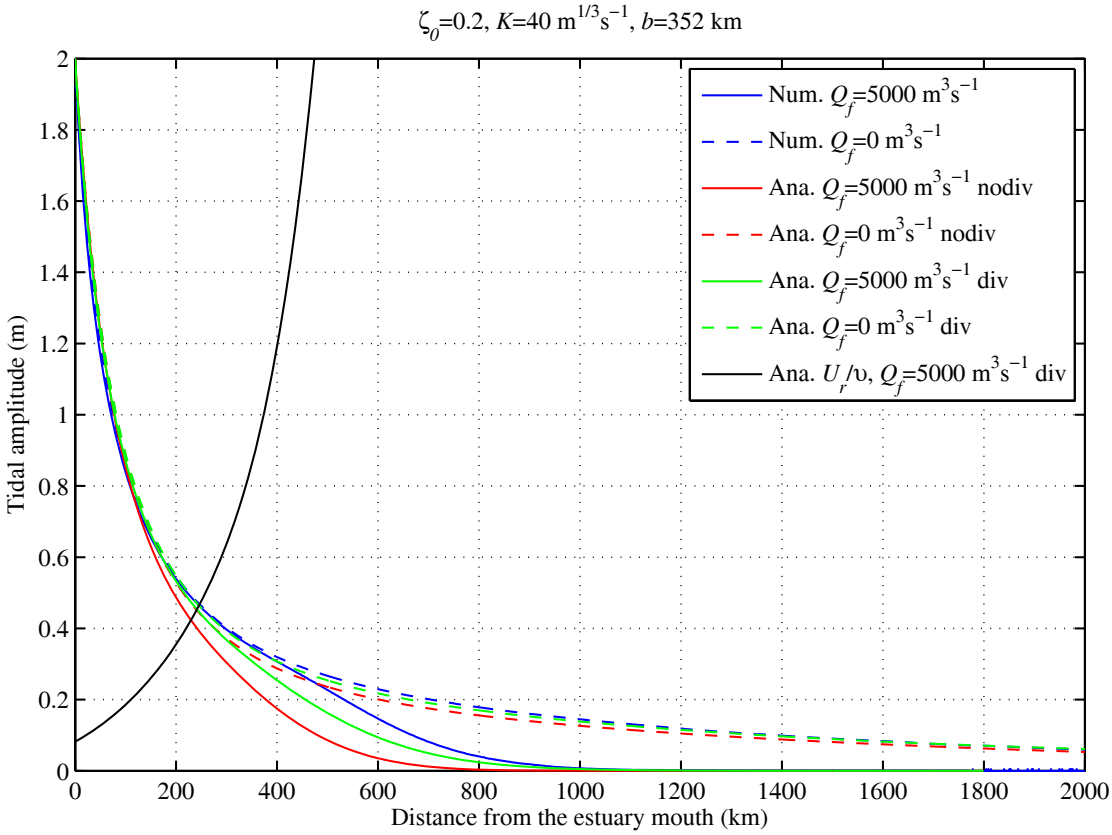

Figure S1. Comparison between different analytical models and numerical results for given values of K=40 m$^{1/3}$s^{-1}, b=352 km, ζ_0=0.2, $\overline{h}$=10 m, $\overline{B_0}$=5000 m, $\overline{B_{\min}}$=300 m. The label "nodiv" indicates the models without considering the residual water level slope, while "div" denotes the models accounting for it using the approach described in Sect. 5.

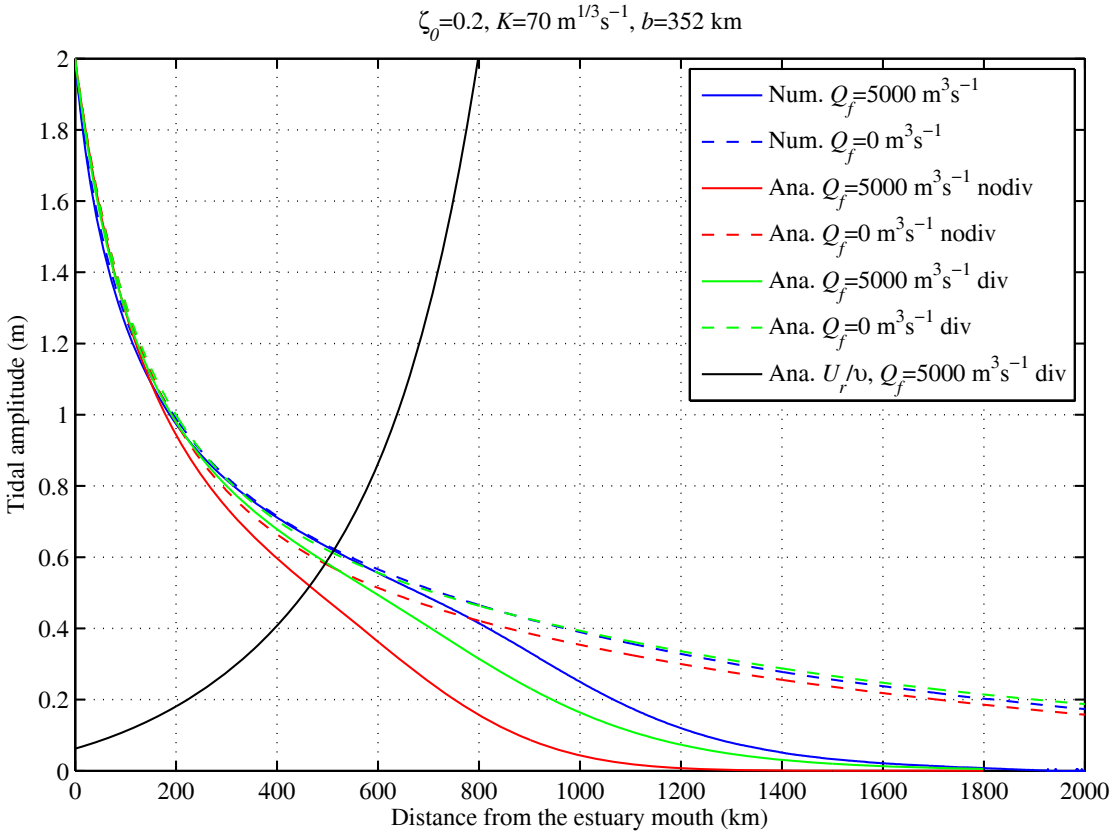

Figure S2. Comparison between different analytical models and numerical results for given values of K=70 m$^{1/3}$s^{-1}, b=352 km, ζ_0=0.2, $\overline{h}$=10 m, $\overline{B_0}$=5000 m, $\overline{B_{\min}}$=300 m. Notation as in Figure S1.

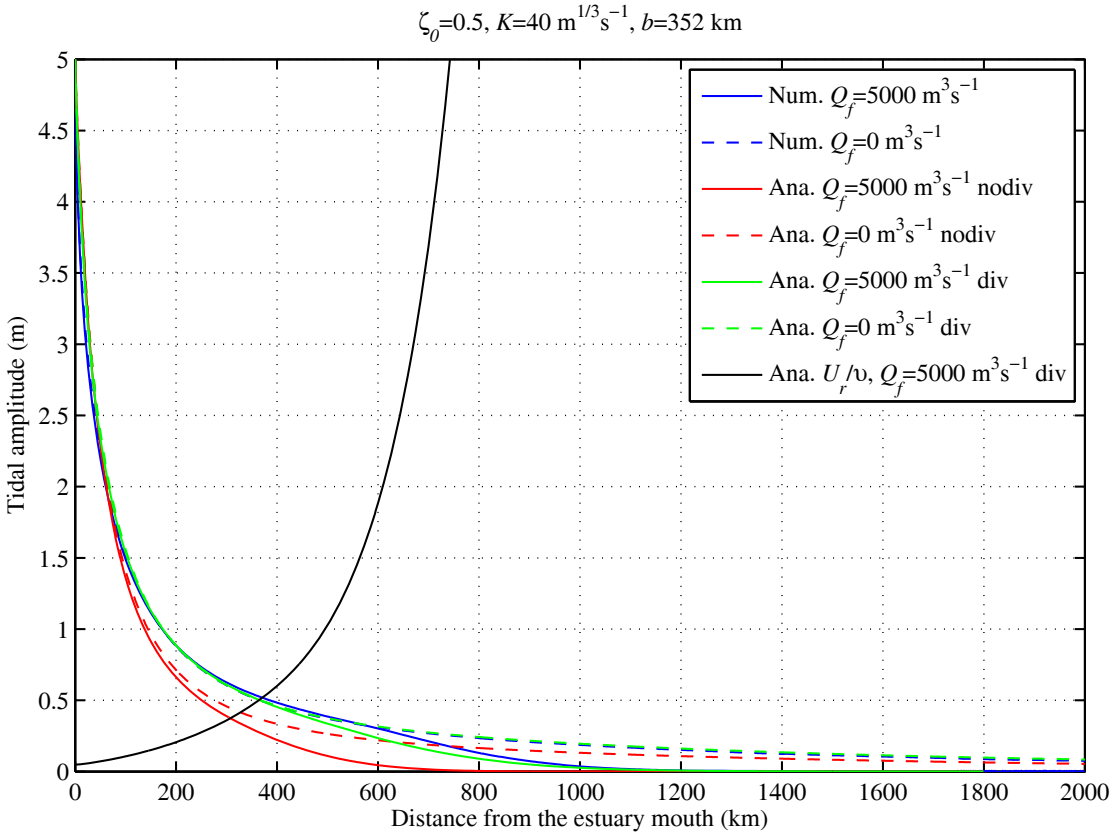

Figure S3. . Comparison between different analytical models and numerical results for given values of K=40 $m^{1/3}s^{-1}$, b=352 km, ζ_0=0.5, $\overline{h}$=10 m, $\overline{B_0}$=5000 m, $\overline{B_{min}}$=300 m. Notation as in Figure S1.

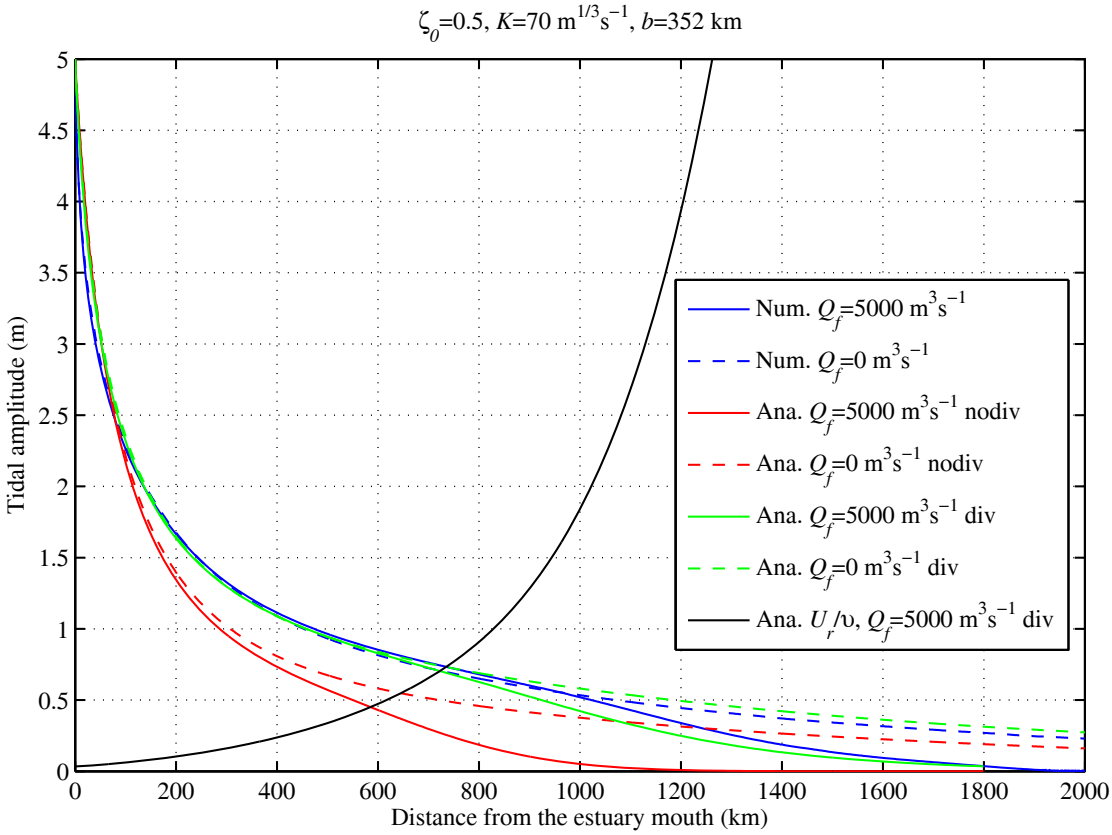

Figure S4. . Comparison between different analytical models and numerical results for given values of K=70 $m^{1/3}s^{-1}$, b=352 km, ζ_0=0.5, $\overline{h}$=10 m, $\overline{B_0}$=5000 m, $\overline{B_{min}}$=300 m. Notation as in Figure S1.

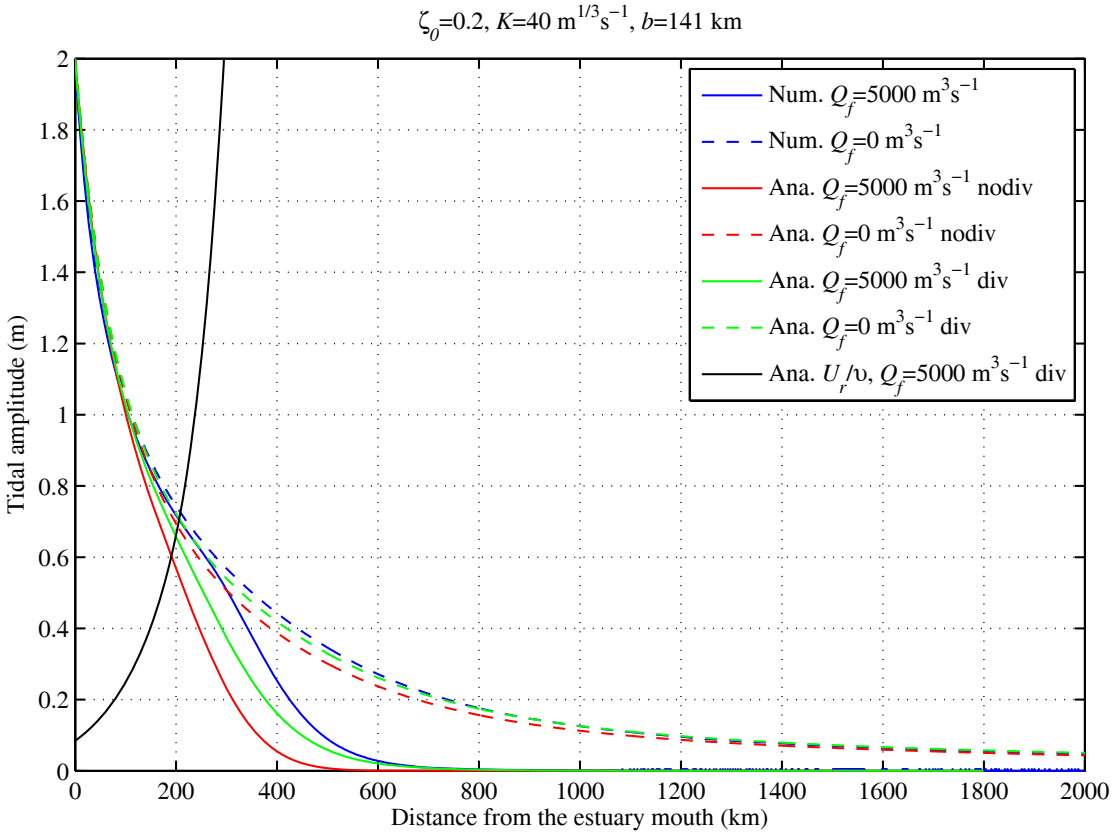

Figure S5. Comparison between different analytical models and numerical results for given values of K=40 m$^{1/3}$s^{-1}, b=141 km, ζ_0=0.2, $\overline{h}$=10 m, $\overline{B_0}$=5000 m, $\overline{B_{\min}}$=300 m. Notation as in Figure S1.

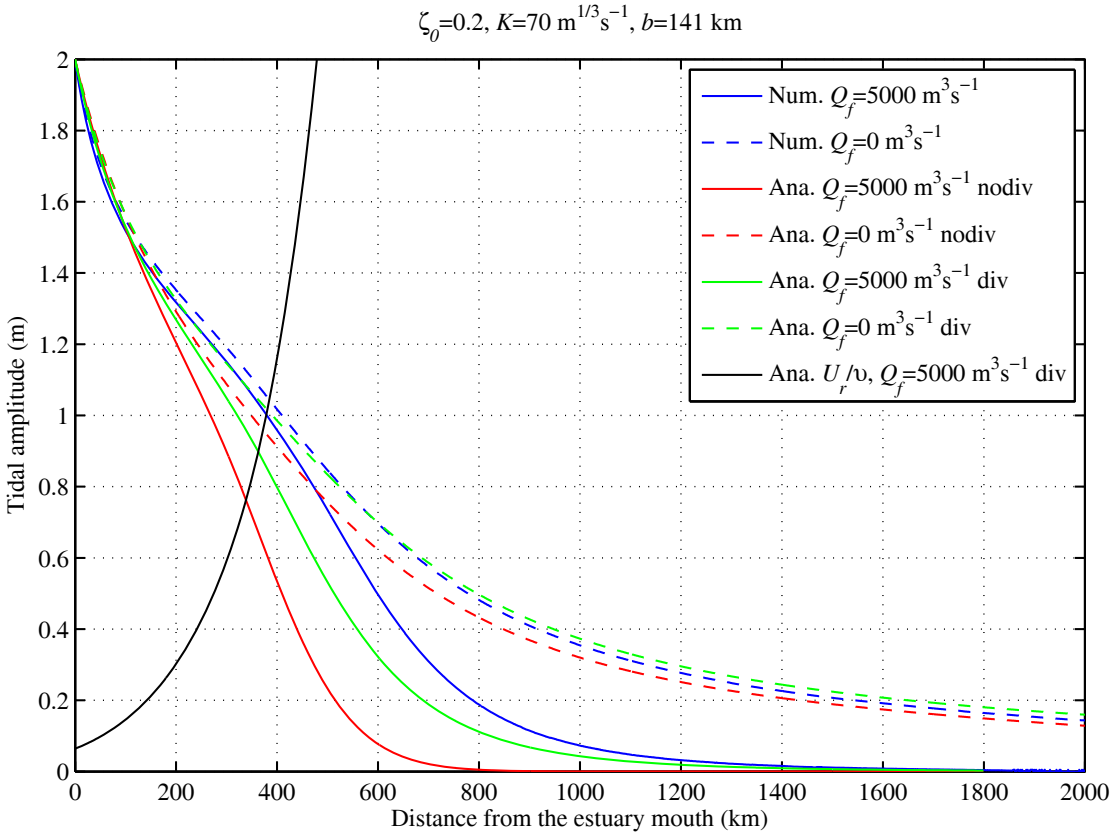

Figure S6. Comparison between different analytical models and numerical results for given values of K=70 $m^{1/3}s^{-1}$, b=141 km, ζ_0=0.2, $\overline{h}$=10 m, $\overline{B_0}$=5000 m, $\overline{B_{min}}$=300 m. Notation as in Figure S1.

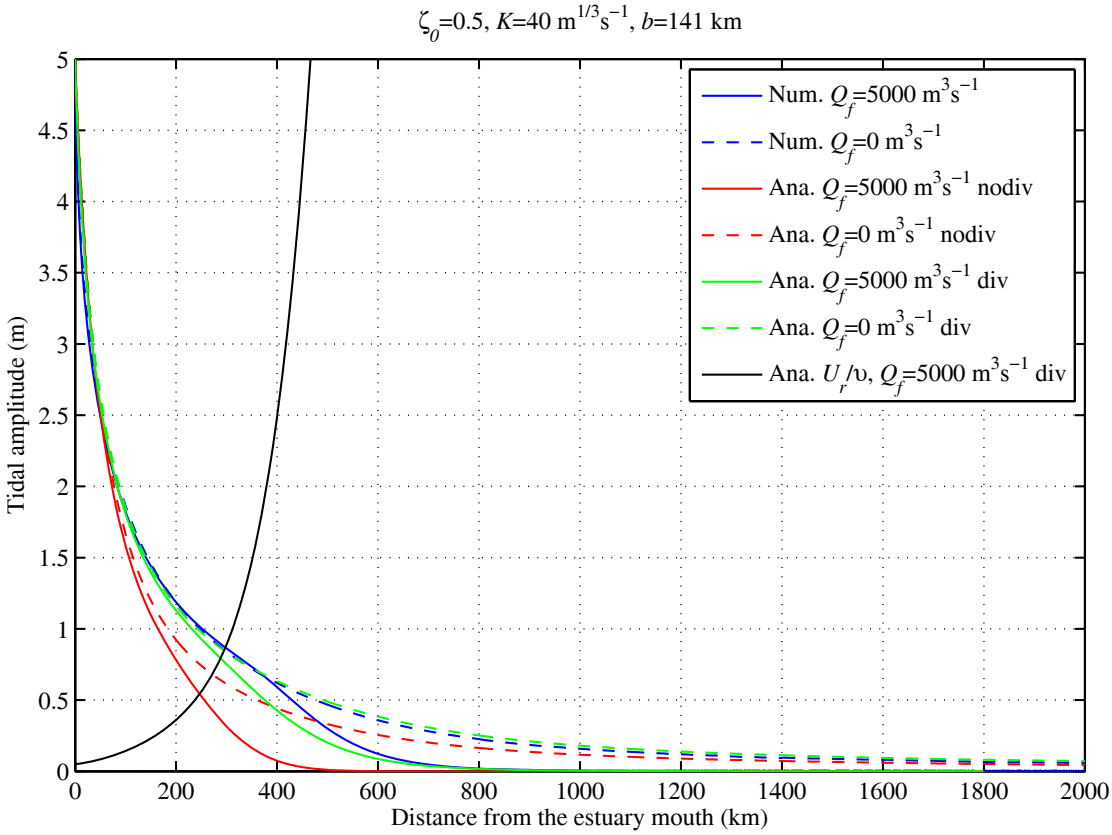

Figure S7. Comparison between different analytical models and numerical results for given values of K=40 $m^{1/3}s^{-1}$, b=141 km, ζ_0=0.5, $\overline{h}$=10 m, $\overline{B_0}$=5000 m, $\overline{B_{min}}$=300 m. Notation as in Figure S1.

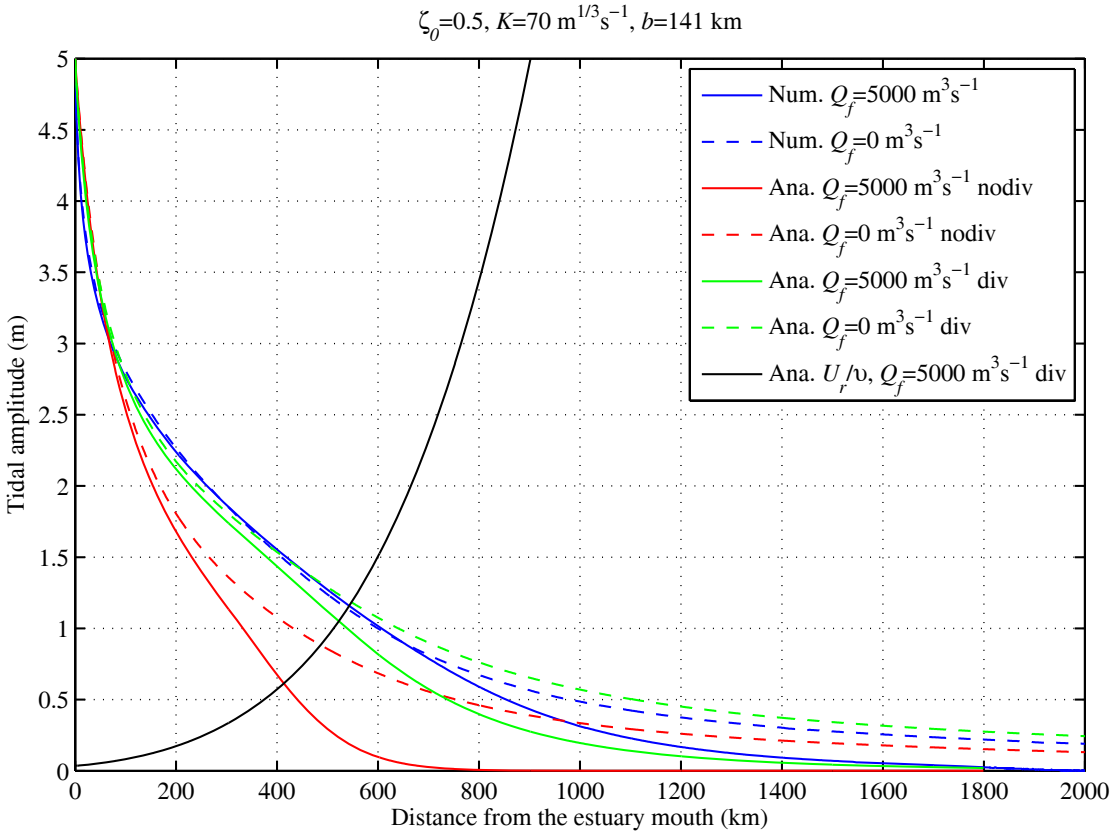

Figure S8. Comparison between different analytical models and numerical results for given values of K=70 m$^{1/3}$s^{-1}, b=141 km, ζ_0=0.5, $\overline{h}$=10 m, $\overline{B_0}$=5000 m, $\overline{B_{\min}}$=300 m. Notation as in Figure S1.